Journal of Anatomy

J. Anat. (2014) **225**, pp152–166 doi: 10.1111/joa.12201

Analysis of joint force and torque for the human and non-human ape foot during bipedal walking with implications for the evolution of the foot

Weijie Wang,[1,2] Rami J. Abboud,[1] Michael M. Günther[3] and Robin H. Crompton[3]

[1]*Department of Orthopaedic and Trauma Surgery, Institute of Motion Analysis and Research, The Ninewells Hospital and Medical School, The University of Dundee, Dundee, UK*
[2]*The School of Mathematics and Physics, Nanjing University of Information Science and Technology, Nanjing, China*
[3]*Institute of Aging and Chronic Disease, The University of Liverpool, Liverpool, UK*

Abstract

The feet of apes have a different morphology from those of humans. Until now, it has merely been assumed that the morphology seen in humans must be adaptive for habitual bipedal walking, as the habitual use of bipedal walking is generally regarded as one of the most clear-cut differences between humans and apes. This study asks simply whether human skeletal proportions do actually enhance foot performance during human-like bipedalism, by examining the influence of foot proportions on force, torque and work in the foot joints during simulated bipedal walking. Skeletons of the common chimpanzee, orangutan, gorilla and human were represented by multi-rigid-body models, where the components of the foot make external contact via finite element surfaces. The models were driven by identical joint motion functions collected from experiments on human walking. Simulated contact forces between the ground and the foot were found to be reasonably comparable with measurements made during human walking using pressure- and force-platforms. Joint force, torque and work in the foot were then predicted. Within the limitations of our model, the results show that during simulated human-like bipedal walking, (1) the human and non-human ape (NHA) feet carry similar joint forces, although the distributions of the forces differ; (2) the NHA foot incurs larger joint torques than does the human foot, although the human foot has higher values in the first tarso-metatarsal and metatarso-phalangeal joints, whereas the NHA foot incurs higher values in the lateral digits; and (3) total work in the metatarso-phalangeal joints is lower in the human foot than in the NHA foot. The results indicate that human foot proportions are indeed well suited to performance in normal human walking.

Key words: finite elements; foot proportions; pressure; simulation; work.

Introduction

In functional and comparative anatomy, we all too often made the assumption that features which looked like they might have adaptive value in some way, did actually enhance performance (Alexander, 1991). A case in point is the evolution of the human foot, our most specialised and unique anatomical structure. The anatomical features seen in modern human feet seem to appear in a piecemeal fashion, and it has recently been proposed that there are different types of mosaic morphologies in the feet of several fossil hominin taxa, and potentially at different lineages with different types of bipedalism (Harcourt-Smith & Aiello, 2004).

Joint shape has long been assumed to be informative about foot function, and indeed the shape of the talar trochlea in the human foot does seem to have a role in permitting a parasagittal path for the lower leg (see e. g. Aiello & Dean, 1990). However, the complexity of the multiple joints formed between the 26 bones of the foot, and their latticework of ligaments and tendons, and the fact that the plantar surface is quite deeply covered with soft tissues, means that joint motion *in vivo*, and even centres of joint rotation, are extremely difficult to determine. Much analysis of the fossil record for the early hominin foot is therefore couched in broadly comparative terms, with individual bones being described as relatively 'human-like' or 'ape-like' (i.e. non-human ape or NHA-like), and the

Correspondence
Weijie Wang, Institute of Motion Analysis and Research, TORT Center, Ninewells Hospital and Medical School, Dundee DD1 9SY, UK. T: + 44 (0)1382 383518; F: + 44 (0) 1382 383501;
E: w.wang@dundee.ac.uk

Accepted for publication *22 April 2014*
Article published online *13 June 2014*

remaining analysis being broadly qualitatively functional or descriptive. For example, Day & Napier (1964) described the most complete foot, *Homo habilis* OH-8 (c. 1.8 MY) as possessing strong longitudinal arches and an unopposable hallux, but with a talus showing a mosaic of human-like and 'ape-like' (i.e. NHA-like) features. Kidd (1995) described OH-8 as 'ape-like' on the medial side (no arch, opposable hallux and mobile, unstabilised talo-navicular joint) but with a markedly 'human-like' (stabilised) calcaneo-cuboid joint on the lateral side. Wood (1974) argued that the KNM ER-813 talus is much more 'human-like' than that of OH-8, suggesting affinity to the (again contemporaneous) striding biped *H. ergaster* (1.8 MY). Harcourt-Smith (2002) described the talus of the Stw 573 foot (*A. africanus*) as 'ape-like', and the navicular as morphologically intermediate between human and ape, but the hallux as 'probably unopposable'.

What is the significance of human-like or ape-like (NHA-like) features? The assumption is clearly made that the human foot is adapted to habitual bipedal walking, as although all apes can and do walk bipedally, only humans are habitual bipeds, so that human-like features mean adaptation to bipedal walking. This has never been tested. In the longer term we need to develop means of analysing the foot as a functional unit, using more objective and quantitative assessments of function. As a first step this paper seeks to advance our understanding of human foot function by testing whether the difference in bone proportions between the feet of different apes, including humans, can be shown to have a quantifiable biomechanical consequence in terms of joint force, torque and work in human-like walking.

An obvious difference between human and NHA feet is in the length of the phalanges, which are relatively short in humans (Schultz, 1963 and see Fig. 1). While the hallux or great toe has similar metatarsal/phalangeal length ratios, the length of the phalanges of the third digit is only 18% of total foot length in humans, but 33% of total foot length in gorillas and 35% in chimpanzees (Keith, 1929). In general, the lengths of the lateral four toes are shorter in humans than in apes (Stern & Susman, 1983; Aiello & Dean, 1990).

Biomechanical analyses of the human foot have dealt with stress and forces on the metatarsals (Arangio et al. 1997; Gefen, 2002), viscoelastic characteristics (Gilchrist & Winter, 1996), muscle behaviour (Alexander, 1977; Reeser et al. 1983; Ker et al. 1987; Alexander et al. 1990; Winter, 1990; Wright et al. 2000; Jacob, 2001) and other topics

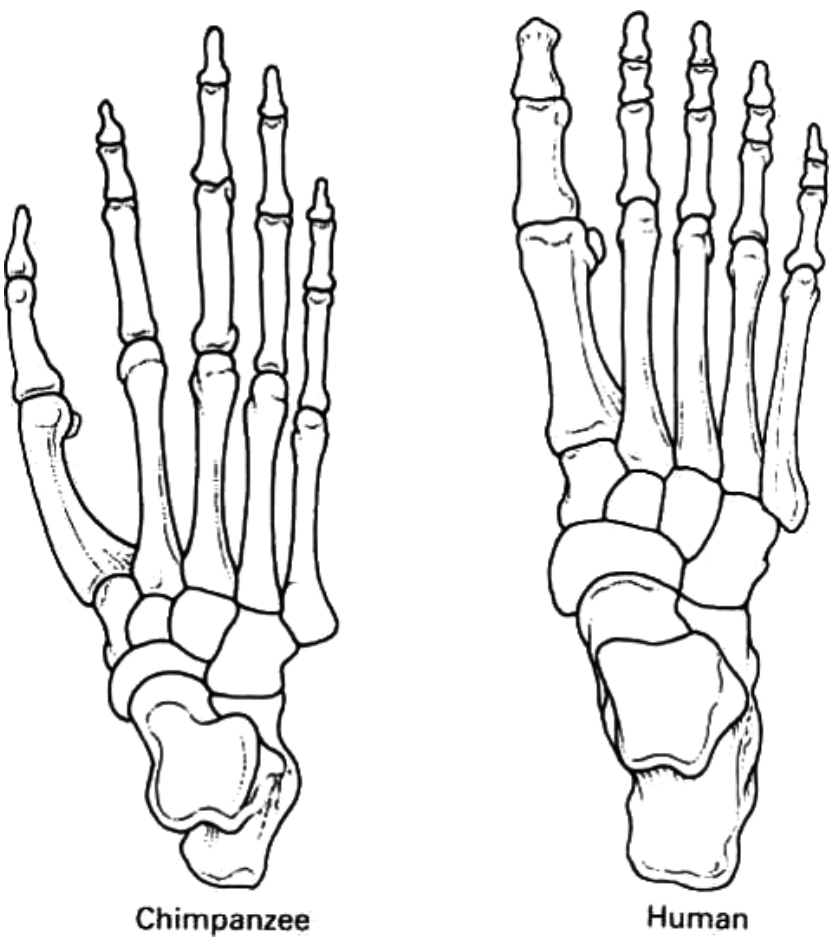

Fig. 1 Comparison of the human and ape foot (from Schultz, 1963). In general, the ape foot has relatively longer metatarsals and phalanges than has the human foot.

(Salathe et al. 1986; Meldrum, 1991; Gebo, 1992; Nigg et al. 1993; Kim & Voloshin, 1995; Wang et al. 1995, 2003a,b, 2004; Cavanagh et al. 1997; Hansen et al. 2001; Bramble & Lieberman, 2004; Wang & Crompton, 2004a). However, few researchers, apart from Preuschoft (1969, 1970) and Stefanyshyn & Nigg (2000), have estimated the important mechanical parameters of joint force, torque and work for the foot of apes. It is therefore these parameters which we shall adopt as our criteria for assessing performance capability.

There are no ethically acceptable means to investigate the internal mechanics of the human or NHA foot other than by modelling and, importantly for our purposes, modelling also enables us to examine the mechanical response of the model to behaviours which the species in question would not perform in nature. Testing human-like walking for other apes would help us to get clues on whether the human foot has been evolved to be suitable for bipedal walking. Human-like bipedal walking is such an activity, although the bipedalism of intensively trained common chimpanzees (Kimura, 1985) and untrained orangutans, and to a much lesser extent bonobos (Crompton et al. 2003), may sometimes approach the activity characteristics of human bipedalism in their own bipedal gaits but only at very low walking speeds. [In Kimura's 1996 study, energy transformation arising from the exchange of kinetic and potential energies during the walking of trained chimpanzees (40% at 0.5 m s^{-1}) fell to zero by 1.6 m s^{-1}].

In a previous modelling study (Wang & Crompton, 2004b), we analysed contact force and muscle force across the foot joints of the human and ape foot during bipedal standing. It was found that the human foot incurs lower joint and muscle forces, indicating that characteristics such as bone proportions and arch height enhance human-like bipedal standing. Here, we address ourselves to dynamic rather than static responses of the foot joints during human-like bipedal walking, given different foot proportions.

Materials and methods

General

Our approach is to represent skeletal proportions of humans, common chimpanzees, gorillas and orangutans by multi-rigid-body (MRB) models, and to model the plantar surfaces of the foot that contact the ground during the gait cycle, by finite element (FE) surfaces. Use of FE surfaces, which can be assigned non-rigid material properties, allows more realistic modelling of ground contact forces than is possible using rigid-body segments alone. The models are then driven by joint motion functions collected from experiments on human walking. After the simulation of models' walking, the joint forces and torques in the foot are produced. To simulate subject walking using rigid-body models, it is assumed that foot muscles and ligaments contribute to joint force, torque and work. In other words, the amount of joint work is related to the activities of the muscles and ligaments around the joint. The more work done and the greater the muscle force expended, the more energy is consumed. We then evaluate the adaptedness of the feet for (human-like) bipedal walking in terms of the mechanical parameters: joint force, torque and work, under the hypothesis that the human foot should perform better in terms of these three parameters.

A limitation of the approach used in this paper is that joint motion is input into the model, not generated by the model itself. In other recent forwards-dynamic modelling studies (e.g. Sellers et al. 2005) we have used genetic-algorithm (GA) evolutionary robotics techniques to derive optimal gaits for a given morphology by a process analagous to natural selection: muscle activation parameters are allowed to mutate over many generations, each generation selecting the best-performing sets (according to given criteria such as distance travelled for a given energetic cost) as the basis of the next generation. Such techniques are computationally highly intensive, and at present computational limitations do not permit modelling of mechanical responses within the foot itself. Moreover, holding kinematics as the same input to all models but comparing morphologically different models is perhaps a more logical approach to answering the question posed here.

Subjects

Skeletons of an adult male chimpanzee, lowland gorilla, orangutan and human in the collection of the Department of Human Anatomy and Cell Biology, University of Liverpool, were selected for measurement. The main dimensions recorded for application to the models are listed in Table 1. The subjects used for experimental analysis were chosen to be as similar as possible in stature to the human skeletal sample. A single specimen of each species was judged sufficient, as we are concerned at this stage only with the effect of the gross difference in morphology between humans and NHAs, and not even the differences among NHAs. To estimate the weights of the whole body and the segments, the principle of similarity is applied (Alexander, 1992) specifically: the ratio of the mass of the subject modelled to that of a known subject is proportional to power 3 of the ratio of the long bone lengths or the statures of the subjects (see Appendix). Standard techniques (Clauser et al. 1969; Jensen, 1989; Nigg & Herzog, 1999; Thorpe et al. 1999) were employed for estimation of rotational inertia and mass distribution. A commercial software package for dynamic analysis of mechanical systems, MADYMO® (TNO, 2001) was employed. MADYMO is unusual in that it permits hybrid FE/MRB modelling, enabling us not only to take advantage of the computational economy of rigid body modelling where this is adequate, but also to model non-rigid material properties where this is desirable, as it is particularly modelling interactions between the soft tissue of the plantar surface of the foot and the ground which are considered. The software was implemented on a 4 processor Silicon Graphics Onyx2 workstation.

The foot

Ideally, the foot model should be a biorealistic model, including accurate 3D geometry and material properties of not only bones and joint surfaces, but all soft tissues. This is at the present moment computationally prohibitive. Even then, *in vivo* joint forces within the foot could not be measured for verification purposes, even if it were ethically acceptable to do so.

For the present, to reduce computational demands to a level where they can be met by existing technology, the bones in the

Table 1 Subjects for modelling and the main characteristic sizes.

	Chimpanzee		Orangutan		Gorilla		Human	
	29		47		58		76	
Weight (kg) Segment	MP	*L*	MP	*L*	MP	*L*	MP	*L*
Head	6.0	0.145	7.3	0.2	8.7	0.19	5.45	0.29
Trunk	54	0.550	50.7	0.4	53.3	0.78	48.8	0.75
Upper arm	3.5	0.280	2.6	0.3	4.2	0.37	2.4	0.30
Arm + hand	4.5	0.47	2.3	0.36	5.0	0.545	2.3	0.45
Thigh	6.4	0.275	10.3	0.3	5.4	0.32	12.2	0.44
Calf	3.51	0.215	4.0	0.28	2.6	0.24	4.8	0.42
Foot	2.0	0.200	1.5	0.26	1.7	0.245	1.2	0.26

MP, mass proportion of total weight; *L*, the characteristic length (m).
When applied to the models, masses and lengths of segments underwent minor modification to facilitate articulation.

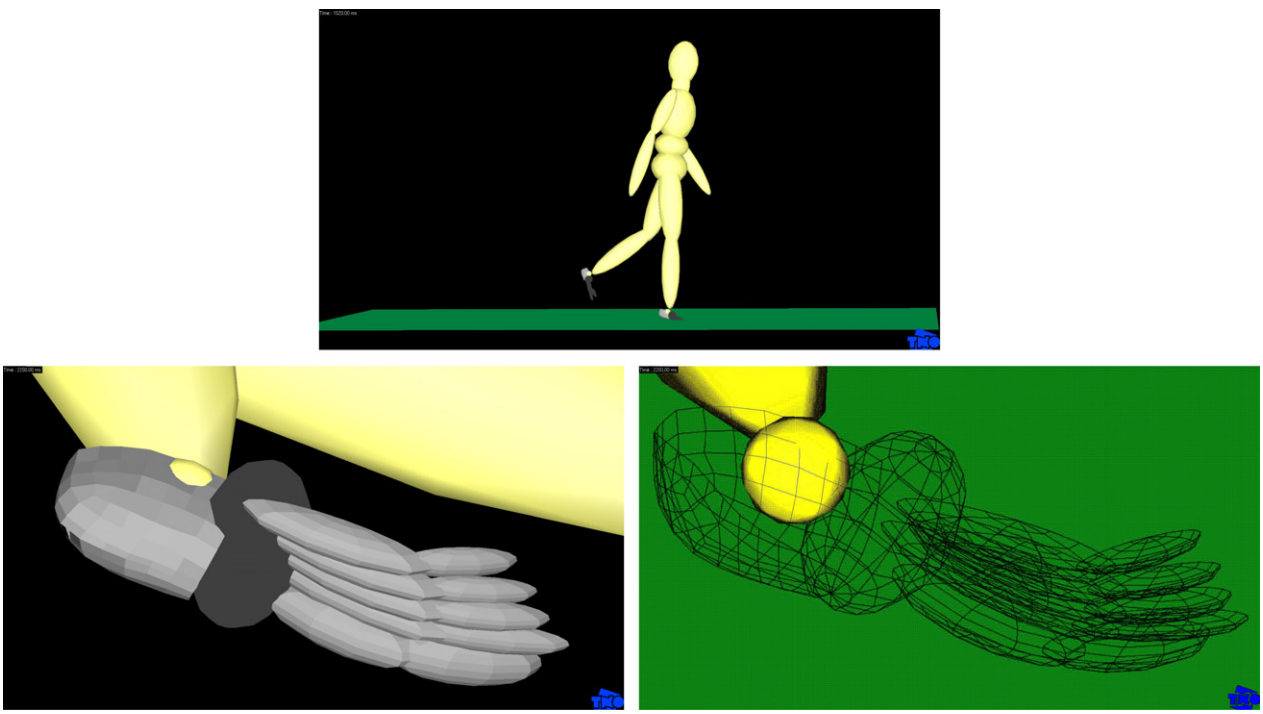

Fig. 2 Above: The whole model. Below: Two more detailed views of the foot model. The whole model is constructed according to measured subject dimensions. The 'bone units' in the foot were built as finite elements surfaces (left). The FE nodes are visible in the figure to the right.

foot were represented by idealised geometrical entities (Fig. 2): the talus as a ball of appropriate diameter, and the navicular, cuneiforms and cuboid as a single ellipsoidal midfoot unit. The five metatarsals were individually represented, but the five sets of phalanges were combined as five single units. Metatarsals and phalangeal units were represented as elliptical semi-spheroids with the convex surface contacting the 'ground'. The 'calcaneus' is represented only by a component modelling the soft tissue surrounding the calcaneus and its contact surface with the ground; this tissue is represented geometrically by a gently curved plantar plate, with a more tightly curved surface representing the proximal, lateral and medial walls. The three main dimensions taken from each actual bone during skeletal measurements (Table 2) were maximum length, width and height, and they were applied appropriately to the geometric entities which represent them. Bone length was defined as the maximum length from the proximal to distal articular surfaces. For ease in representing the bone measurements as simplified FE surfaces, the maximum medial-lateral dimension (width) and inferior-superior dimension (height) at the proximal end of the bones were taken as the lengths of the two shorter axes for the FE models. For clarity we shall henceforth describe the simulated foot components as 'bone units', as their FE surfaces have compliant material properties simulating the action of the plantar soft tissues.

Table 2 The detailed dimensions of the bones in the models (cm).

	Chimpanzee			Orangutan			Gorilla			Human		
Bone	*L*	*W*	*H*	*L*	*W*	*H*	*L*	*W*	*H*	*L*	*W*	*H*
Calcaneus	4.6	3.0	4.0	6.8	6.0	6.0	7.3	3.6	3.3	8.0	2.5	2.5
Talus	3.8	2.7	2.0	3.2	3.3	3.3	3.0	4.5	3.8	3.5	3.3	3.6
Cuneiform	2.2	3.7	2.0	3.0	4.8	2.5	3.0	4.8	2.0	4.0	6.5	3.2
Metatarsal1	4.8	1.5	1.8	6.5	1.5	2.0	4.7	1.8	2.3	6.0	2.0	3.0
Metatarsal2	6.2	1.2	1.3	11.5	1.5	2.0	7.1	1.5	1.9	7.5	1.5	1.8
Metatarsal3	6.2	1.2	1.4	11.5	1.5	2.0	6.7	1.4	2.0	6.8	1.4	2.0
Metatarsal4	5.9	1.0	1.2	15.0	1.4	2.0	6.5	1.1	1.5	6.8	1.4	2.0
Metatarsal5	5.7	1.6	0.9	10.0	1.8	1.5	7.3	1.3	1.3	6.8	1.5	2.0
Phalanx 1	4.15	1.0	0.8	5.5	1.5	1.1	3.9	7.5	1.2	5.7	2.0	1.5
Phalanx 2	7.2	0.9	0.8	7.2	1.5	1.5	7.4	1.2	1.2	6.0	1.2	1.0
Phalanx 3	7.0	0.9	0.8	7.8	1.5	1.8	6.7	1.3	1.1	5.1	1.2	1.2
Phalanx 4	5.8	0.9	0.8	7.8	1.6	1.6	6.2	1.2	1.2	4.8	1.1	1.0
Phalanx 5	5.5	0.8	0.7	0.6	1.4	1.4	5.7	1.0	1.0	4.7	1.2	1.0

L, length in the longitudinal axis of bone; *W,* width in the medial-lateral direction at the proximal end of bone; *H,* height in the inferior-superior direction; unit (cm). These dimensions were obtained from measurement of the skeletons and used to construct the finite element representations of the bones and their surrounding soft tissue.

Mesh dimensions ranged from 66 nodes for the contact surface of each of the metatarsals or phalangeal bone units, to 200 nodes for the calcaneal bone units. During simulation of walking, the FE mesh contacts the ground (the latter being modelled as a rigid body), and the contact produces stresses are then summed to produce the ground reaction forces (GRFs) that support and drive the whole-body model during walking.

The foot bone units, as well as the rigid segments representing the rest of the body, were assigned mechanical characteristics including mass and inertia. The whole foot mass was estimated from the data in the literature (Clauser et al. 1969; Jensen, 1989; Nigg & Herzog, 1999; Thorpe et al. 1999). To obtain the mass and moment of inertia for each bone units, the proportion of the mass of individual bones to the mass of the whole foot skeleton was used to distribute the total mass of the intact foot among bone units. Rotational inertias of the 'bone units' were estimated (Appendix) from the idealised geometries. Since the study was intended to predict joint forces and torques within the foot during the stance phase of gait only, errors in estimation of the mass distributions for the foot should not influence reliability excessively. Mass distribution would have a much more substantial effect in the swing-phase foot.

Joints

The joints represented in the 'upper body' were the talo-crural, knee, hip, gleno-humeral and humero-ulnar. In the foot, the joints represented were the subtalar, the talo-navicular (here linking the talus and the midfoot element), the tarso-metarsal joints (between the midfoot unit and the metatarsals) and the metatarso-phalangeal joints between the metatarsals and the single-unit phalanges. The subtalar and the talo-navicular joints were not assigned freedom to move due to being fixed by the ligaments, and thus served only for calculation of joint forces. As the model was only free in the sagittal plane (despite having three-dimensional geometry and area contacts with the ground), all joints were therefore defined as revolute. A joint with 3 degrees of freedom (translational in the anterior-posterior and vertical directions, and rotational around a medial-lateral axis) was assumed to exist, linking the lower trunk of the model to the global reference system. All mobile joints between segments were driven by motion functions obtained from experiments on human walking. The mechanical parameters for the ground and the FE surfaces of the foot, such as the coefficient of friction and the values of damping, are shown in Table 3.

Table 3 Mechanical parameters used for modelling.

Contact-type	Friction	Damping	Hysteresis-slope
Stress	0.5–1.2	40–90	1.0E + 5 – 1.0E + 8

These parameters are described in the MADYMO Theory Manual (see Supporting Information for details).

Contact between ground and foot

To simulate the compliance of the soft tissue of the plantar surface of the foot, energy-absorbing functions were provided for the contact between the foot and the ground, employing a hysteresis model. The functions require specification of a loading curve, an unloading curve, a hysteresis slope and an elastic limit (see MADYMO manual, TNO, 2001). Related parameters have been listed in Table 3.

Driving the model

To drive the model in walking, and for model verification purposes respectively, kinematic data were collected from experiments on human normal walking. A male adult (height 175 cm, 40 years old and weight 76 kg) undertook a set of trials. The subject was required to walk barefoot at a self-determined comfortable speed through an experimental volume covered by four high-speed (200 Hz) digital area-scan cameras, and across

an a 0.5-m pedobarographic platform (RSscan® Footscan 2001) mounted on a force platform (Kistler® 9821B, Kistler Instrumenti, 1995). Software integration (using commercially available RSSCAN FOOTSCAN software) ensured that the pressure platform output was continuously recalibrated by the Kistler platform's output for the superimposed presence of the plate. The digital images from the four area-scan cameras were captured to disk using twin two-channel Raptor digital capture cards and the recorded sequences were then digitised by the purpose-written in-house software (Wang, 1999) to obtain the motion functions for the major joints (humero-ulnar, gleno-humeral, hip, knee, talo-crural and metatarso-phalangeal) that were to be applied to the simulations. Prior to the experiments, the dorsum of the subject's feet was marked with a rectilinear grid and the cameras were set as close as possible to the pressure/force platform combination so as to obtain reasonably accurate motion functions for the foot joints from deformation of the grid (see Fig. 3A–C).

Optimisation algorithm

Provided with the data described above for the models, and the single set of motion functions to be applied to them, the MADYMO software has the information required to drive our models. As a result, joint forces and torques can be obtained. However, as MADYMO is designed for the automotive industry and could not itself generate stable, smooth bipedal walking. Therefore an algorithm was developed specifically for the simulation of bipedal walking, in which mathematical optimisation and parameter adjustment are applied to the search for biologically reasonable solutions for the simulations (Wang, 1999). In brief, the algorithm searches for possible optimum solutions for problems of multi-variable dynamic simulation. The variables, which were adjusted during optimum search, included the contacting parameters in Table 3 and the initial walking velocity at the beginning when a model starts walking. Mechanically, these variables are called boundary conditions and are sensitive to model posture during simulated walking. During searching, the range of variables is first divided into finite points, and during the progress of searching, their range is progressively reduced until biologically satisfactory solutions are obtained (i.e. the model can walk upright for two cycles). In early solutions, the models may fall, roll or jump rather than walk. Such solutions are progressively eliminated from the search area. Finally, a limited set of optimum solutions can be obtained and the models can simulate stable human-like walking. In the previous studies (Wang et al. 2002; Wang & Crompton, 2004a), the algorithm proved capable of obtaining reasonable solutions for simulations of normal human walking. The algorithm has been further improved for the purposes of this paper, particularly with respect to analysis of the foot (see Fig. 4 and Supporting Information).

To verify the results obtained by the algorithm, simulated vertical ground reaction force curves (vGRFs) for the optimised solutions were compared with experimentally recorded values for the same performance (i.e. that for which the motion functions used were derived). Similarity or difference of two curves could in theory be assessed statistically or using artificial-intelligence (AI) techniques such as pattern recognition. Neither could or should eliminate human judgment. However, from our own previous studies (e.g. Li et al. 1996; Crompton et al. 1998; Wang et al. 2003b) and those of other authors (e.g. Vereecke et al. 2003, 2005), the range of vGRF curves obtainable during normal human bipedal walking, as opposed to that exhibited by great apes, is well documented. Curves from normal human bipedal walking have two humps or peaks and a steep rise and fall at first and last ground contact of the stance phase, respectively. In most but not all cases, voluntary bipedalism of other apes produces a single plateau (i.e. flat hump or peak) in mid-stance, a variable rise time at first contact, but nearly universally a long tail (i.e. a slowly decreasing trend) during the last phase of contact. Walking by some flat-footed humans may produce vGRF curves resembling those of apes (RSscan, pers. comm), whereas bipedally walking orangutans and, less often, bonobos may produce vGRF curves similar to those produced by humans in slow walking. There is thus a considerable area of overlap between human and NHA vGRF curves in bipedal walking, but the *characteristic* features of human vGRF curves are well known and these were required to be present in predicted vGRF curves for the respective simulations to be regarded as successful. We did *not* expect simulated vGRF curves to have identical magnitudes, as magnitudes vary considerably between speeds and iterations by the same human individual. Neither did we expect performances free of artefacts such as noise, or additional but transitory peaks or spikes, which are known to result from the inevitably poorer damping in any model constructed even partially from rigid-body segments.

Joint parameters

To evaluate foot performance, joint force and torque was obtained. The method by which work and torque were calculated is summarised in the Appendix. In addition, to compare different models in terms of the cost of transport, the work done at the metatarsophalangeal joints during walking was calculated and normalised by body weight and the distance traveled by the centre of mass over a cycle of walking. The parameter reflects how much mechanical work is required in the foot joints to drive walking.

Results

Simulated vGRFs are shown in Fig. 5. As the simulated walking was stable over two cycles, and simulated vGRFs were reasonably comparable with experimentally obtained values (according to the criteria we have stated above), the method used for dynamic simulation is regarded as reliable (see the Supporting Information for the videos on the models walking stably for two cycles).

Model verification against measured vGRF curves

From the simulations, we can obtain not only the total vGRF of the whole foot but also the contributory vGRFs for each component of the foot (see Fig. 5). The patterns of the total vGRF are similar to data output by the Kistler force platform, and the simulated vGRFs for each component of the foot are, in the same way, comparable with the data simultaneously output by the superimposed RSscan pressure plate. (As force platforms such as the Kistler measure point forces, they cannot provide partitioned vGRFs, which must be obtained from local pressures using a pressure transducer such as the RSscan Footscan system). To the best of our knowledge, this study is the first to have been able to predict forces under the foot partitioned between different basic regions.

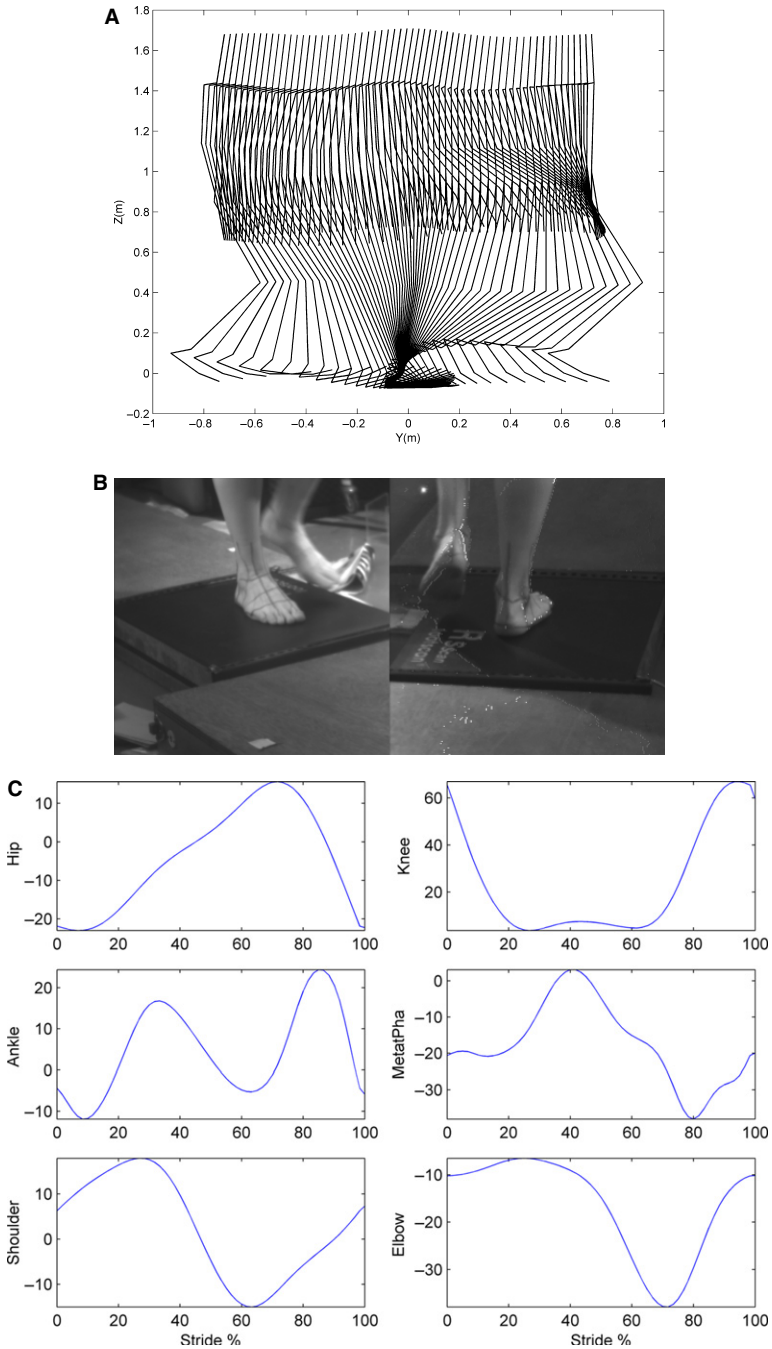

Fig. 3 (A) A stick-figure representation of the input motion for normal human walking. Data was obtained by 3D reconstruction from images from four digital area scan cameras at 200 Hz. Motion functions were derived from this sequence for each joint and used as input data to drive the model's joints in walking simulations. (B) The collection of kinematic data on the foot during walking. Grids marked on the dorsal surface of the foot give data on internal motion of the foot and the reference frames for digitisation of images. (C) The joint angles (degrees) applied in the simulation of the models. Data was obtained from experiments on normal human walking; and the motion functions used to drive the joints of the model in simulations of walking.

Normalisation

The averages of joint forces and torques during the stance phase of a cycle of walking were calculated and compared. As the subjects were different in weight and stature, the results were normalised before comparisons were made. In the normalisation, simulated joint forces were divided by the body weight of the subject and the joint torque divided by the product of body weight and leg length (Figs 6 and 7). In most biomechanical studies, either leg length or height is used in normalisation. As NHAs had a non-straight posture which made it difficult to measure height, we used their leg length to normalise the torques. We discuss and compare merits and disadvantages of different normalisation techniques elsewhere (Wang & Crompton, 2004b).

Joint force and torque

From Figs 6 and 7, it can be seen that NHA models have different distributions of joint forces and torques from the human model. As the magnitude of the vertical component of the GRF vector is always far greater than its horizontal

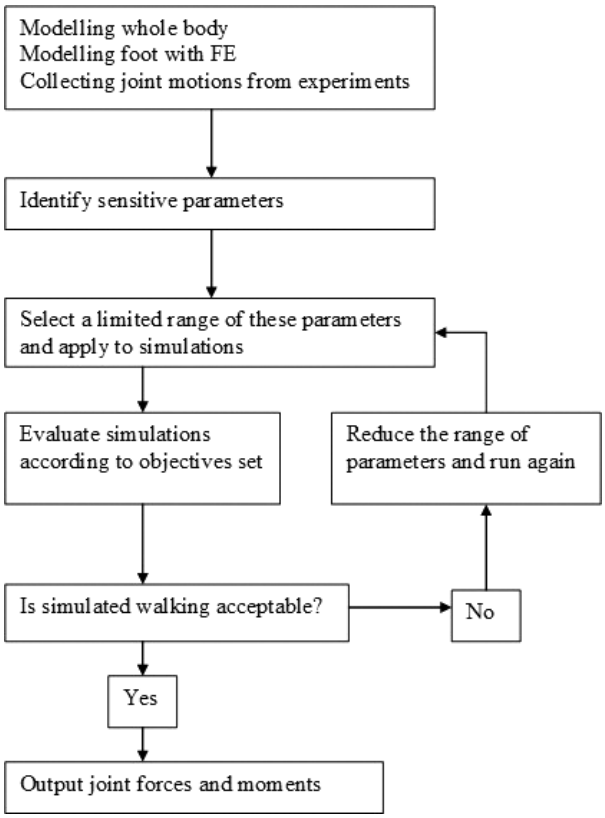

Fig. 4 Flowchart of modelling and optimisation algorithm: Level 1: skeletal elements are measured to obtain dimensions for the models; the foot 'bone units' are constructed using finite elements; joint motion is collected from experiments on human walking; the computer model is built using MADYMO. Level 2: Identify sensitive parameters. Level 3: Select a limited range of these parameters and apply to simulations. Levels 4 and 5: Evaluate simulations according to objectives set. If walking simulated is acceptable, output joint forces and moments, if not: reduce the range of parameters and run again.

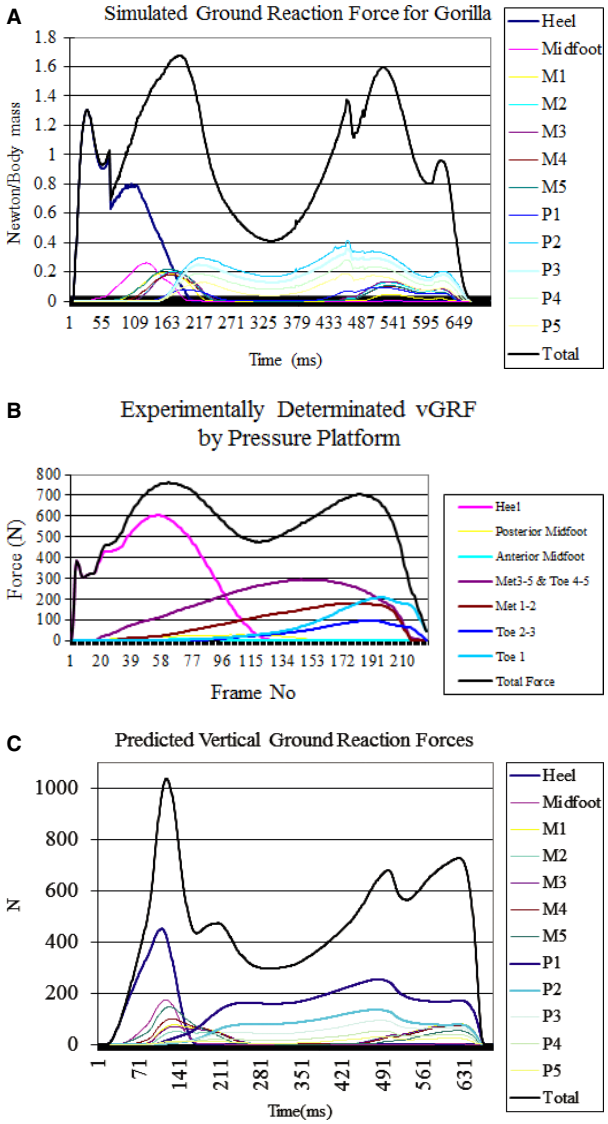

Fig. 5 (A) The simulated vertical ground reaction forces (vGRFs) for the gorilla simulation. From the simulation, we plot not only the total of vGRFs (the double-humped curve with higher values than other curves) but also sub-vGRFs for each component of the foot (other curves). M1 to M5 represent the first to fifth metatarsals and P1 to P5 the first to fifth phalanges. (B) Vertical ground reaction forces (vGRFs) for total foot and individual foot regions as recorded using a pressure platform. vGRF curves for each region have reasonably similar patterns to simulated values (see Fig. 5C). Met1-2 are the first and second metatarsals, and Met3-5 the third to fifth metatarsals. (C) Predicted vGRFS for whole foot and different regions derived from simulations. vGRF curves have reasonably similar patterns to measured values (compare Fig. 5B). 'Heel' represents the calcaneus; 'M1 to M5' the first to fifth metatarsals, 'P1–P5' the first to fifth phalanges and 'Midfoot' the navicular, cuboid and cuneiforms.

component, the latter may be ignored for the present purpose of comparing joint torques. Considering the sagittal plane through each joint, at any instant, the ground reaction force vector can be either posterior or anterior to the instant centre of a joint, depending on gait. Let us assume that the subject moves from right to left. When the vGRF vector lies posterior to the instant centre of the joint, the torque produced will then be anti-clockwise, but when it lies anterior to the joint, torque will be clockwise. Similarly, in the coronal (frontal) plane, when the vGRF occurs lateral to a joint, the torque produced will have a rotational direction from the lateral, to the medial side of the joint; and when the vGRF acts on the medial side of a joint, the torque will be from medial to lateral. In this study, the quantity of a torque is considered more important than the direction. The higher the quantity, the more the muscles/ligaments areinvolved around the joint.

The results show that the human foot incurs greater joint force and torque in the first tarso-metatarsal and the first metatarso-phalangeal joints, whereas the feet of NHAs incur higher values in the lateral four joints. This may be attributed to two factors, different bone proportions and movement functions. Humans have relatively long and

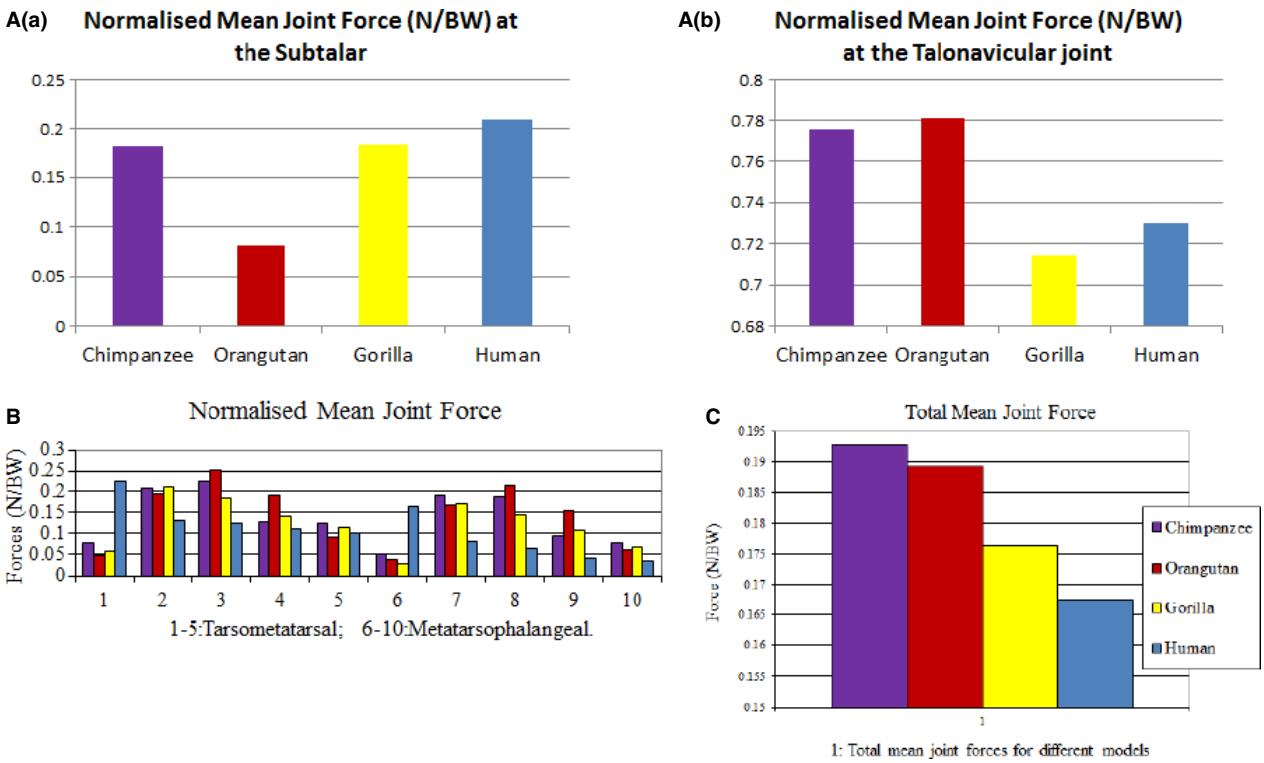

Fig. 6 (A) Comparison of the normalised mean joint force during a cycle of walking. (Left, top) The subtalar joint between the talus posterior section and calcaneus. (Right, top) The 'talo-navicular' joint between the talus and the midfoot. (B) Comparison of the normalised mean forces in the foot joint during a cycle of walking. Numbers 1–5 represent the first to fifth tarso-metatarsal joints, respectively, and numbers 6–10 the first to fifth metatarso-phalangeal joints, respectively. (C) Comparison of the total means for all joint forces in the foot joint during a cycle of walking. The results show that the human foot has total mean joint force similar to that of the feet of NHAs. (Note that values on the vertical axis have a small range).

robust hallucial metatarsals and hallucial phalanges, whereas NHAs have relatively long and robust metatarsals and phalanges in the lateral four digits. As functions from human-like bipedal walking are used in the simulations, they reflect in particular, and hence act to emphasise, the propulsive role of the hallucial metatarsal and phalanges during toe-off.

The different performance of the human and NHA feet draws attention to relationships between foot proportions and mechanical action. A robust 'bone units' will result in high joint force, as force acting on the bone is the product of the force under the bone and the area over which the 'bone unit' contacts the ground. Thus joint force is mainly determined by the area of the 'bone unit' in contact with the ground. However, joint torque is the product of the lever length (the moment arm, e.g. the distance from the joint centre to the GRF) and the forces acting on the joint centre (e.g. the GRF). Sometimes, therefore, although joint force is large, joint torque may not be particularly high, as lever length is not great. This is the case in the human foot, where simulated mean torques are less than those for NHA feet, although simulated mean joint forces in the human foot are similar in magnitude to those in NHA feet.

Joint work

The results show that the total work done during walking in all foot joints studied is higher in the feet of NHA simulations than in the foot of the human simulation. The distribution of work has a similar pattern to that of torque (see Fig. 8).

Discussion

Joint force

Total averages of the normalised joint forces in all subjects studied have similar values, at around 0.17–0.19 N BW^{-1} (Newtons divided by body weight) (Fig. 6C). Totals of joint force are thus not markedly different between the human foot and that of the NHAs. The distributions of joint forces are, however, quite different. The human model incurs relatively large forces in the first tarso-metatarsal and first metatarso-phalangeal joint, whereas NHA models incur relatively great forces in the lateral four digits. As only the proportions of the models vary, these distinctions must result from their different proportions, and most likely the proportions of the foot. It is the gorilla which, according to

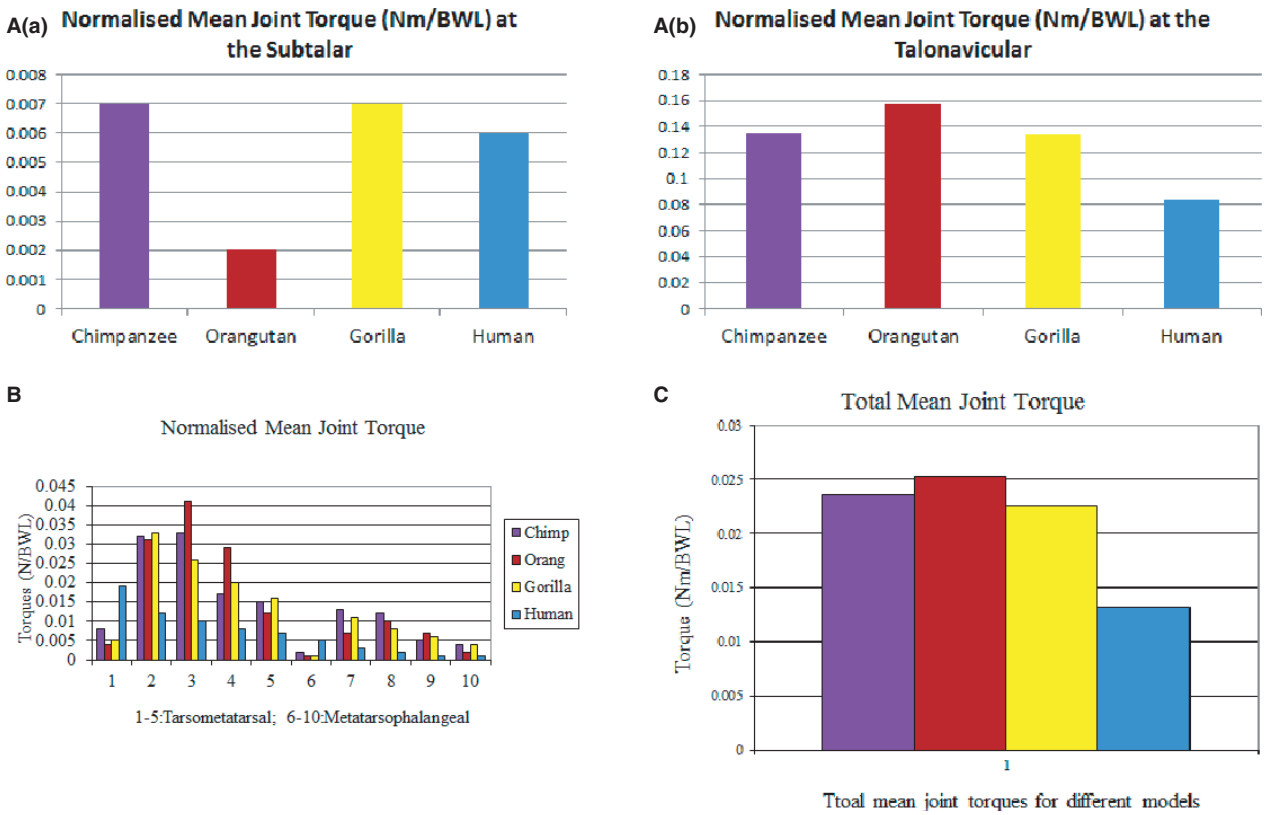

Fig. 7 (A) Comparison of the normalised mean torques in the foot joints during a cycle of walking. (Left, top) The subtalar joint. (Right, top) The 'talo-navicular' joint between the talus and the midfoot. (B) Comparison of the normalised mean torques in the foot joint during a cycle of walking. Numbers 1–5 represent the first to fifth metatarsal joints, respectively, Numbers 6–10 the first to fifth metatarso-phalangeal joints respectively. (C) Comparison of the total mean joint torques in the foot during a cycle of walking. The human foot has a lower total mean than do the NHA feet.

our results, most resembles humans in terms of mean joint force and mean joint torque; and it is the gorilla, too, which resembles humans in having a long tarsus and short lateral phalanges (Schultz, 1963; Tuttle, 1970): the phalanges of the third digit are about 33% of foot length versus 43% in *Pongo* and 35% in *Pan troglodytes*.

Joint torque and work

Comparing average joint torques, it is evident that in our simulations of human-like walking, joints in the feet of NHA subjects bear larger torques than do joints in the human foot. The overall means of normalised joint torque in the apes are 0.024 Nm BWL^{-1}*** (Newton metres divided by body weight and leg length) for the common chimpanzee, 0.025 for the orangutan and 0.023 for the gorilla, but only 0.013 for the human model (Fig. 7C). In other words, simulated joint torques in the NHA feet are about 1.8 times greater than in the simulated human foot. The external torques are mainly balanced by the forces/moments exerted about the joints by muscles and ligaments. Therefore, the higher joint torque in NHA feet implies that during performance of human-like bipedal walking, muscles and ligaments of NHAs would have to bear larger loads/greater tension, increasing the risk of injury. Work requirements of the NHA models were much higher than those in the human (Fig. 8) and in reality this would increase mechanical

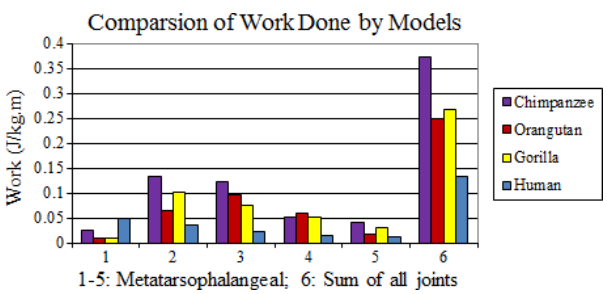

Fig. 8 Comparison of the work done at the metatarso-phalangeal joints in the models. The joint work is calculated using the product of the joint torques and angular displacements during a cycle of walking, and then normalised by the body mass and the distance travelled by the centre of mass over a cycle of walking. Numbers 1–5 represent the first to fifth metatarso-phalangeal joints, Number 6 the total work done in all joints. The total work done at the five joints is less in the human foot than in the NHA feet, although the work in the first metatarso-phalangeal joint is greater in the human foot than in that of NHAs.

(and hence metabolic) energy costs. To produce more energy, there would in turn be an adaptive requirement to increase the physiological cross-sectional area (PCSA) of muscles. Moreover, higher joint torque would apply larger bending moments to the foot bones, and thus increase stress inside the bones, leading to an adaptive requirement to enlarge bone diameter. Foot mass, in turn, would have to increase and so, in turn, would the rotational inertia about the major joints, such as the ankle, the knee and the hip.

Robusticity of the first digit is of obvious relevance to the toe-off phase of human bipedal walking, as the human toe-off phase has high vertical forces and is sustained for long periods, and that thrust is applied more anteriorly in humans, under the metatarsal heads and on the phalanges of the first digit, rather than under the midfoot (Vereecke et al. 2003, 2005). Medial rotation of the thigh, transferred to the forefoot via the medial and lateral malleoli, talus and navicular in the 'closed kinematic chain', ensures that as final thrust is applied, the body centre of mass lies fairly close to the plane of the stance hallux. The shortness of the lateral toes reduces joint torque, but also the weight of the foot, and moments of inertia. Given that the motion functions applied to all models were derived from human bipedalism, the relatively large force and torque in the first tarso-metatarsal and the first metatarso-phalangeal joints of humans may be brought about by a combination of: (i) the robusticity of the hallucial metatarsal and phalanges, (ii) the contribution the position of the hallucial tarso-metatarsal joint makes to angulation against the ground of the hallucial metatarsal, and hence to formation of the medial longitudinal arch, and of course (iii) the role the first metatarsal and phalanges play in supporting and transferring loads.

Limitations of this study

As we have noted, the morphology of the foot-models used in this study was by no means biorealistic. Idealised geometric shapes (e.g. ellipsoids, spheroids) had to be used, primarily not only to reduce computational load, but also to avoid noise due to irregular ground contacts (given the relative lack of compliance of the foot model). Ideally, we would use a foot which modelled both the form and the material properties of bones, muscles, ligaments, tendon, connective tissue and skin accurately, and which took into consideration joint shape and the guiding action of ligaments during stance. Various attempts have been made to do so (e.g. Gurfinkel et al. 1994) but a biorealistic model is still a long-term goal of biomechanicists. It is striking, however, that even such a simplified foot model as we have used can produce a simulation of the pattern of the forces under the various regions of the foot.

We have also noted that using human-walking functions in the models is one of the limitations, and we would like to apply the motion functions of other apes to the models. To obtain the bipedal motion functions from great apes, we spent nearly a whole year in a zoo, setting up a motion capture system to monitor chimpanzees and orangutans and any possible bipedal walking, but we failed to collect even one completed/perfect cycle. In almost all of the collected cases, the chimpanzees and orangutans were moving in 'tri-pedal walk', i.e. with two feet and a hand on the ground. In literature, there has been little research reporting a completed set of motion functions, including lower and upper limbs for other apes. In the future, the models could be tested using NHA motion functions if available.

Another limitation is that the subtalar, talo-navicular, and midtarsal joints were not assigned freedom to move. Movements at these joints certainly contribute to foot function in NHAs (as well as to the closed kinematic chain in the human foot) and are of particular importance to the NHA midtarsal break (Susman, 1983). From a broader perspective it would thus have been better if they had been incorporated in the NHA foot models. A broader comparative study of foot function in the great apes would of course require inclusion of all such factors, and would enable us, for example, to examine the mechanical response of human morphology to motion functions derived from the locomotion of other apes. However, the difficulty of obtaining high-resolution joint motion data for apes other than humans would pose great challenges to such studies.

Comparison with other methods

In addition to being able to partition forces under the foot, we regarded it as important in this study to require that simulations were stable over several cycles of walking. Most other such studies (e.g. Mugnai et al. 1998; Jonkers et al. 2002) have simulated only half a cycle, and indeed doing so reduces computational demands on optimisation to such an extent that Nagano et al.'s (2005) forwards dynamics model could be three-dimensional (see also discussion in Sellers et al. 2005). Sampling only a half-cycle risks missing instants of major change in joint force and torque. Again, we have regarded it as important to model the whole body rather than treat the upper body as a particle or single unit (e.g. Neptune et al. 2001; Jonkers et al. 2002). Further, unlike another of our own recent modelling studies (Sellers et al. 2005) our present model considers not only the mass and inertia of the trunk, the head and upper limbs, but also the relative motion of the shoulders and elbow joints. In actual human walking, the motion of the upper limb does influence contact forces under the foot, and hence must exert an indirect influence on joint force (Li et al. 2001). The present generation of computational technology thus forces us to choose to concentrate on some aspects of biorealism at the expense of others. The next generation(s) may well free us from that unwelcome choice.

Recently, FE models have been used to investigate foot behaviour in walking. Qian et al. (2013) employed the ankle force to drive an FE foot and obtained GRF similar to the device-measured ones; however, they did not calculate joint forces for other joints, or simulate multi-part GRF distribution under the foot. Yu et al. (2013) estimated the pressures at the metatarsophalangeal (MTP) joints but did not validate the model using multi-part foot pressure or joint forces for other joints. In fact, all previous studies focused on some aspects of the FE foot models, e.g. heel pressure (Gu et al. 2011; Luo et al. 2011) and landing impact (Cho et al. 2009; Natali et al. 2010), rather than considering the whole body and multi-parts in the foot during walking. The model provided in this study is unique because it employs a whole subject body with the multi-rigid-body, multi-joint and multi-surface foot. As a pilot study, the model was applied to the apes but has potential to be applied to other fields, e.g. sports and ergonomics, in the near future.

Conclusion

The significance of this study is threefold. First, it has shown that proportions of the feet in humans and apes exert a discernible effect on joint force, torque and work in the foot, even within a whole-body context, and confirms what was previously only an assumption, that the proportions of human feet are dynamically more advantageous for human-like bipedal walking than those of apes. Secondly, in doing so, we have shown that short toes play an important functional role in human walking. Thirdly, we have shown that the form of contact forces between the foot and the ground can be predicted not only for the foot as a whole but also for the basic functional units of the foot. This implies that a fully three-dimensional model should be able to predict the path of the centre of pressure, and the development of pressure over the contact surfaces under the foot. Simulation of the dynamics of early hominid feet, based on their proportions, and eventually including biologically accurate bone form, joint shape, ligamentous guiding and control, muscles, connective tissue and skin, should then enable a quantitative assessment of their performance effectiveness in different behaviours.

Acknowledgements

There is no conflict of interest to our knowledge. This research has been supported by the Leverhulme Trust, the Biotechnology and Biological Sciences Research Council, and the Natural Environment Research Council, UK. This study was partially supported by the funds from the Department of Orthopaedic and Trauma Surgery, University of Dundee, the Joint Project of the Royal Society of Edinburgh and National Natural Science Foundation of China, and Ministerio de Ciencia e Innovación CGL2010-20868 of Spain.

References

Aiello L, Dean C (1990) *An Introduction to Human Evolutionary Anatomy*. London: Academic Press, pp. 507–538.

Alexander RMN (1977) Terrestrial locomotion. In: *Mechanics and Energetics of Animal Locomotion* (eds Alexander RMN, Goldspink G), pp. 168–201, London: Chapman and Hall Ltd.

Alexander RMN (1991) Apparent adaptation and actual performance. *Evol Biol* **25**, 357–373.

Alexander RMN (1992) Mechanics of animal locomotion. *Advances in Comparative and Environmental Physiology*, Vol. 11. London: Springer-Verlag.

Alexander IC, Chao E, Johnson KA (1990) The assessment of dynamic foot-to-ground contact forces and plantar pressure distribution – a review of the evolution of current techniques and clinical-applications. *Foot Ankle* **11**, 152–167.

Arangio GA, Xiao D, Salathe EP (1997) Biomechanical study of stress in the fifth metatarsal. *Clin Biomech* **12**, 160–164.

Bramble DL, Lieberman DE (2004) Endurance running and the evolution of *Homo*. *Nature* **432**, 345–352.

Cavanagh PR, Morag E, Boulton AJM, et al. (1997) The relationship of static foot structure to dynamic foot function. *J Biomech* **30**, 243–250.

Cho JR, Park SB, Ryu SH, et al. (2009) Landing impact analysis of sports shoes using 3-D coupled foot-shoe finite element model. *J Mech Sci Technol* **23**, 2583–2591.

Clauser CE, McConville JT, Young JW (1969) *Weight, Volume, and Center of Mass of Segments of the Human Body*. AMRL Technical Report (TR-69-70). Dayton, OH: Wright-Patterson Air Force Base.

Crompton RH, Li Y, Wang WJ, et al. (1998) The mechanical effectiveness of erect and 'bent-knee, bent-hip' bipedal walking in *Australopithecus afarensis*. *J Hum Evol* **35**, 55–74.

Crompton RH, Thorpe S, Wang WJ, et al. (2003) The biomechanical evolution of erect bipedality. *Courier Forschungsinstitut Senckenberg* **243**, 135–146.

Day MH, Napier JR (1964) Fossil foot bones. *Nature* **201**, 969–970.

Gebo DL (1992) Plantigrady and foot adaptation in African apes – implications for hominid origins. *Am J Phys Anthropol* **89**, 29–58.

Gefen A (2002) Stress analysis of the standing foot following surgical plantar fascia release. *J Biomech* **35**, 629–637.

Gilchrist LA, Winter DA (1996) A two-part, viscoelastic foot model for use in gait simulations. *J Biomech* **29**, 795–798.

Gu YD, Li JS, Lake MJ, et al. (2011) Image-based midsole insert design and the material effects on heel plantar pressure distribution during simulated walking loads. *Comput Methods Biomech Biomed Eng* **14**, 747–753.

Gurfinkel VS, Ivanenko YP, Levik YS (1994) The contribution of foot deformation to the changes of muscular length and angle in the ankle joint during standing in man. *Physiol Res* **43**, 371–377.

Hansen MI, Otis JC, Kenneally SM, et al. (2001) A closed-loop cadaveric foot and ankle loading model. *J Biomech* **34**, 551–555.

Harcourt-Smith WEH (2002) Form and function in the hominoid tarsal skeleton. PhD Thesis. London: University College London.

Harcourt-Smith WEH, Aiello LC (2004) Fossils, feet and the evolution of human bipedal locomotion. *J Anat* **204**, 317–432.

Jacob HAC (2001) Forces acting in the forefoot during normal gait – an estimate. *Clin Biomech* **16**, 783–792.

Jensen RK (1989) Changes in segment inertial proportions between 4 and 20 years. *J Biomech* **22**, 529–536.

Jonkers I, Spaepen A, Papaioannou G, et al. (2002) An EMG-based, muscle driven forward simulation of single support phase of gait. *J Biomech* **35**, 609–619.

Keith A (1929) The history of the human foot and its bearing on orthopaedic practice. *J Bone Joint Surg* **11**, 10–32.

Ker RF, Bennett MB, Bibby SR, et al. (1987) The spring in the arch of the human foot. *Nature* **325**, 147–149.

Kidd RS (1995) An investigation into patterns of morphological variation in the proximal tarsus of selected human groups, apes and fossils: a morphometric analysis. PhD Dissertation. Perth, WA, Australia: The University of Western.

Kim W, Voloshin AS (1995) Role of plantar fascia in the load-bearing capacity of the human foot. *J Biomech* **28**, 1025–1033.

Kimura T (1985) Bipedal and quadrupedal walking of primates: comparative dynamics. In: *Primate Morphophysiology, Locomotor Analysis and Human Bipedalism*. (ed. Kondo S), pp. 81–105, Tokyo: University of Tokyo Press.

Kimura T (1996) Centre of gravity of the body during the ontogeny of chimpanzee bipedal walking. *Folia Primatol* **66**, 126–136.

Kistler Instrumenti (1995) *9821B Force Platform Manual*. Winterthur: Kistler Instrumenti.

Li Y, Crompton RH, Gunther MM, et al. (1996) Characteristics of ground reaction forces in normal and chimpanzee-like bipedal walking by humans. *Folia Primatol* **66**,137–159.

Li Y, Wang WJ, Crompton RH, et al. (2001) Free vertical moments and transverse forces in human walking and their role in relation to arm swing. *J Exp Biol* **204**, 47–58.

Luo G, Houston VL, Garbarini MA, et al. (2011) Finite element analysis of heel pad with insoles. *J Biomech* **44**, 1559–1565.

Meldrum DJ (1991) Kinematics of the cercopithecine foot on arboreal and terrestrial substrates with implications for the interpretation of hominid terrestrial adaptations. *Am J Phys Anthropol* **84**, 273–289.

Mugnai A, Oggero E, Pagnacco G, et al. (1998) Human foot modeling: a new approach using Madymo. Presentation at a Madymo user's Meeting, the Netherlands.

Nagano A, Umberger BR, Marzke MW, et al. (2005) Neuromusculoskeletal computer modeling and simulation of upright, straight-legged, bipedal locomotion of *Australopithecus afarensis* (A.L. 288-1). *Am J Phys Anthropol* **126**, 2–13.

Natali AN, Forestiero A, Carniel EL, et al. (2010) Investigation of foot plantar pressure: experimental and numerical analysis. *Med Biol Eng Compu* **48**, 1167–1174.

Neptune RR, Kautz SA, Zajac FE (2001) Contributions of the individual ankle plantar flexors to support, forward progression and swing initiation during walking. *J Biomech* **34**, 1387–1398.

Nigg BM, Herzog W (1999) *Biomechanics of the Musculo-Skeletal System*. West Sussex, UK: John Wiley & Sons Ltd, pp. 380–382.

Nigg BM, Cole GK, Nachbauer W (1993) Effects of arch height of the foot on angular motion of the lower-extremities in running. *J Biomech* **26**, 909–916.

Preuschoft H (1969) Statische Untersuchungen an den Fussen der Primaten. Teil I: Statik der Zehen und des Mittelfusses. *Z Anat Entwicklungsgesch* **129**, 285–345.

Preuschoft H (1970) Statische untersuchungen an den Fussen der primaten. Teil II: Statik des ganzen Fusses. *Z Anat Entwicklungsgesch* **131**, 156–192.

Qian Z, Ren L, Ding Y, et al. (2013) A dynamic finite element analysis of human foot complex in the sagittal plane during level walking. *PLoS ONE* **8**, e79424.

Reeser LA, Susman RL, Stern JT (1983) Electro-myographic studies of the humanfoot – experimental approaches to hominid evolution. *Foot Ankle* **3**, 391–407.

Salathe EP Jr, Arangio GA, Salath EP (1986) A biomechanical model of the foot. *J Biomech* **19**, 989–1001.

Schultz AH (1963) The relative lengths of the foot skeleton and its main parts in primates. *Symp Zool Soc Lond* **1**, 199–206.

Sellers WI, Cain G, Wang WJ, et al. (2005) Stride lengths, speed and energy costs in walking of *Australopithecus afarensis*: using evolutionary robotics to predict locomotion of early human ancestors. *J R Soc Interface* **2**, 431–442.

Stefanyshyn DJ, Nigg BM (2000) Influence of midsole bending stiffness on joint energy and jump height performance. *Med Sci Sports Exerc* **32**, 471–476.

Stern JT, Susman RL (1983) The locomotor anatomy of *Australopithecus afarensis*. *Am J Phys Anthropol* **60**, 279–317.

Susman RL (1983) Evolution of the human foot: evidence from Plio-Pleistocene hominids. *Foot Ankle* **3**, 365–376.

Thorpe SKS, Crompton RH, Gunther MM, et al. (1999) Dimensions and moment arms of the hind- and fore-limb muscles of common chimpanzees (*Pan troglodytes*). *Am J Phys Anthropol* **110**, 179–199.

TNO (2001) *MADYMO: A Dynamic Modeling Software Package, Version 6.0.* Delft, the Netherlands: TNO Automotive.

Tuttle R (1970) Capabilities in the cheiridia of chimpanzees and other apes. In: *The Chimpanzee* (ed. Bourne GH), pp. 167–253, Basel: Karger.

Vereecke E, D'Août K, De Clercq D, et al. (2003) Dynamic plantar pressure distributions during terrestrial locomotion of bonobos (*Pan paniscus*). *Am J Phys Anthropol* **120**, 373–383.

Vereecke E, D'Août K, Van Elsacker L, et al. (2005) Functional analysis of the gibbon foot during terrestrial bipedal walking: planar pressure distributions and three-dimensional ground reaction forces. *Am J Phys Anthropol* **128**, 659–669.

Wang WJ (1999) The mechanics of bipedalism in relation to load-carrying: biomechanical optima in hominid evolution. PhD Thesis. The University of Liverpool.

Wang WJ, Crompton RH (2004a) The role of load-carrying in the evolution of modern skeletal proportions. *J Anat* **204**, 417–430.

Wang WJ, Crompton RH (2004b) Analysis of the human and ape foot during bipedal standing with the implications for the evolution of the foot. *J Biomech* **37**, 1831–1836.

Wang CI, Cheng CK, Chen CW, et al. (1995) Contact areas and pressure distributions in the subtalar joint. *J Biomech* **28**, 269–279.

Wang WJ, Crompton RH, Gunther MM, et al. (2002) A method to determine the optimum solution in multi-variable dynamic simulation, and a preliminary application to human walking. In: *The Engineering of Sport 4* (eds Ujihashi S, Haake SJ), pp. 339–345, Oxford, UK: Blackwell Publisher.

Wang WJ, Crompton RH, Li Y, et al. (2003a) Optimum ratio of upper to lower limb lengths in hand-carrying of a load under

the assumption of frequency coordination. *J Biomech* **36**, 249–252.
Wang WJ, Crompton RH, Li Y, et al. (2003b) Energy transformation during erect and 'bent-hip, bent-knee' walking by humans with implications for the evolution of bipedalism. *J Hum Evol* **44**, 563–579.
Wang WJ, Crompton RH, Carey TS, et al. (2004) Comparison of inverse-dynamics musculo-skeletal models of AL 288-1 *Australopithecus afarensis* and KNM-WT 15000 *Homo ergaster* to modern humans, with implications for the evolution of bipedalism. *J Hum Evol* **47**, 453–478.
Winter DA (1990) *Biomechanics and Motor Control of Human Movement*. New York: John Wiley & Sons Inc, pp. 98–99.
Wood BA (1974) A *Homo* talus from East Rudolf, Kenya. *J Anat* **117**, 203–204.
Wright IC, Neptune RR, van den Bogert AJ, et al. (2000) The influence of foot positioning on ankle sprains. *J Biomech* **33**, 513–519.
Yu J, Cheung JTM, Wong DWC, et al. (2013) Biomechanical simulation of high-heeled shoe donning and walking. *J Biomech* **46**, 2067–2074.

Supporting Information

Additional Supporting Information may be found in the online version of this article:

Video S1. Human model in walking.
Video S2. Orangutan model in walking.
Fig. S1. The explanation on the optimisation algorithm.
Data S1. Madymo manual related pages.

Appendix

Similarity scaling

$$\text{Mass}_{\text{mod}} = \text{Mass}_{\text{sub}} \left(\frac{L_{\text{mod}}}{L_{\text{sub}}} \right)^3$$

where Mass is the mass of the whole body or a segment and L the stature or the length of bone. When the mass of a live subject (the subscript sub) is given, the mass of the model (the subscript mod) can be estimated.

Calculation of work done

$$\text{Work} = \sum_{i=1}^{n} |M_i \cdot \mathrm{d}\alpha_i|$$

where M is the torque (Nm) and $\mathrm{d}\alpha$ the angular change (rad) at the same joint, i the frame number, and n the number of frames for a cycle of gait.

Calculation of joint torque

$$M = \sum F_i \times r_i$$

where M is the torque (Nm) at the joint; and F_i is the force at the ith node in a finite element surface and r_i the distance from the node to the joint.

Table A1 Mass (kg) and inertia (kg m^2) of the limb and foot segments used in modelling.

Segment	Mass	Ixx	Iyy	Izz
Human				
LOTORSO	11.2	0.0989	0.0906	0.114
SPINE	2.29	0.0156	0.0086	0.0234
UPTORSO	23.9	0.476	0.35	0.295
NECK	1.02	0.0017	0.002	0.0025
HEAD	4.29	0.0204	0.0233	0.0151
UPARM	1.9	0.0125	0.0132	0.0025
LOARM	1.84	0.0297	0.0296	0.0017
UPLEG	9.57	0.0297	0.0296	0.0017
LOLEG	3.77	0.0573	0.0582	0.0066
Talus	0.163088	4.71E-05	4.97E-05	4.57E-05
Calcaneus	0.321054	4.86E-05	2.73E-04	2.73E-04
Cuneiform	0.177537	1.13E-04	5.64E-05	1.25E-04
Metat1	0.0787469	1.24E-05	4.29E-05	3.81E-05
Metat2	0.0321489	2.14E-06	2.31E-05	2.28E-05
Metat3	0.0279626	2.02E-06	1.70E-05	1.63E-05
Metat4	0.0330844	2.39E-06	2.01E-05	1.93E-05
Metat5	0.0358816	2.71E-06	2.18E-05	2.11E-05
Pha1	0.0330844	2.50E-06	1.39E-05	1.46E-05
Pha2	0.0130505	3.85E-07	5.84E-06	5.91E-06
Pha3	0.0102533	3.57E-07	3.41E-06	3.41E-06
Pha4	0.0093177	2.49E-07	2.71E-06	2.73E-06
Pha5	0.0097902	2.89E-07	2.74E-06	2.79E-06
Chimpanzee				
LOTORSO	5	0.0271	0.0271	0.02556
SPINE	0.336	0.0056	0.0056	0.00056
UPTORSO	10	0.14	0.14	0.05112
NECK	0.2	0.0017	0.002	0.0025
HEAD	1.704	0.00251592	0.00251592	0.00251592
UPARM	0.994	0.00547261	0.00547261	5.47E-05
LOARM	1.278	0.00431426	0.00431426	4.31E-05
UPLEG	1.8176	0.00965285	0.00965285	9.65E-05
LoLEG	0.99684	0.00323589	0.00323589	3.24E-05
Talus	0.127346	1.74E-05	2.84E-05	3.35E-05
Calcaneus	0.342568	1.04E-04	1.54E-04	1.25E-04
Cuneiform	0.101033	2.16E-05	1.08E-05	2.27E-05
Metat1	0.080429	5.34E-06	2.56E-05	2.46E-05
Metat2	0.0600238	2.27E-06	2.91E-05	2.90E-05
Metat3	0.0646411	2.66E-06	3.16E-05	3.12E-05
Metat4	0.043938	1.30E-06	1.93E-05	1.90E-05
Metat5	0.0509383	2.08E-06	2.05E-05	2.16E-05
Pha1	0.0206037	4.09E-07	4.45E-06	4.54E-06
Pha2	0.0321716	5.64E-07	2.04E-05	2.05E-05
Pha3	0.0312779	5.49E-07	1.88E-05	1.89E-05
Pha4	0.025916	4.55E-07	1.07E-05	1.08E-05
Pha5	0.0191143	2.61E-07	7.11E-06	7.14E-06

Table A1. *(continued)*

Segment	Mass	Ixx	Iyy	Izz
Gorilla				
LOTORSO	10	0.116	0.116	0.116
SPINE	0.914	0.0156	0.0086	0.0234
UPTORSO	20	0.58	0.58	0.232
NECK	0.2	0.0017	0.002	0.0025
HEAD	5.046	0.0127922	0.0127922	0.000127922
UPARM	2.436	0.0234192	0.0234192	0.000234192
LOARM	2.9	0.0133083	0.0133083	0.000133083
UPLEG	3.132	0.0225223	0.0225223	0.000225223
LOLEG	1.508	0.0060998	0.0060998	6.10E-05
Talus	0.178924	7.51E-05	5.07E-05	6.33E-05
Calcaneus	0.302476	8.73E-05	2.35E-04	2.42E-04
Cuneiform	0.100449	3.29E-05	1.58E-05	3.89E-05
Metat1	0.0678655	7.00E-06	2.25E-05	2.08E-05
Metat2	0.0705756	5.00E-06	4.61E-05	4.50E-05
Metat3	0.0654311	4.72E-06	3.87E-05	3.71E-05
Metat4	0.0374066	1.57E-06	2.01E-05	1.97E-05
Metat5	0.0430289	1.76E-06	2.86E-05	2.86E-05
Pha1	0.0122422	2.97E-07	2.47E-06	2.34E-06
Pha2	0.037166	1.30E-06	2.53E-05	2.53E-05
Pha3	0.0334166	1.17E-06	1.86E-05	1.88E-05
Pha4	0.031139	1.09E-06	1.50E-05	1.50E-05
Pha5	0.0198804	4.81E-07	8.06E-06	8.06E-06
Orangutan				
LOTORSO	7	0.038	0.038	0.0038
SPINE	2.829	0.0156	0.0086	0.0234
UPPE_TORSO	14	0.076	0.076	0.0076
Neck	0.431	0.0017	0.002	0.0025
HEAD	3	0.0055	0.0055	0.00055
UPPARM	1.222	0.0029	0.0029	0.00029
LOWARM	1.081	0.00156	0.00156	0.000156
UPLEG	4.841	0.012	0.012	0.0012
LOLEG	1.88	0.00042	0.0042	0.0042
Calcaneus	0.456264	2.06E-04	2.35E-04	2.35E-04
Talus	0.0610738	7.85E-06	7.85E-06	7.85E-06
Cuneiform	0.0670977	1.23E-05	6.42E-06	1.35E-05
Metat1	0.0363446	1.42E-06	1.05E-05	1.01E-05
Metat2	0.064302	2.52E-06	5.49E-05	5.42E-05
Metat3	0.064302	2.52E-06	5.49E-05	5.42E-05
Metat4	0.0547965	2.05E-06	3.93E-05	3.86E-05
Metat5	0.0503233	1.73E-06	3.23E-05	3.26E-05
Pha1	0.0169142	3.67E-07	3.34E-06	3.45E-06
Pha2	0.030194	8.52E-07	1.02E-05	1.02E-05
Pha3	0.0392522	1.35E-06	1.58E-05	1.55E-05
Pha4	0.0372169	1.19E-06	1.48E-05	1.48E-05
Pha5	0.0219186	5.39E-07	5.22E-06	5.22E-06

All segment names are abbreviated. When a segment moment of inertia was not known exactly, an estimate has been given. As the study focuses on the analysis of the foot only during the stance phase of walking, such estimation should not overly influence results.